J Mar Sci Technol (2016) 21:190–202
DOI 10.1007/s00773-015-0342-1

ORIGINAL ARTICLE

A finite pointset method for the numerical simulation of free surface flow around a ship

Yu Lu[1] · **An-kang Hu**[1,2] · **Ya-chong Liu**[1]

Received: 20 January 2015 / Accepted: 7 September 2015 / Published online: 24 September 2015

Abstract In this paper, we present a Finite pointset method (FPM) for the numerical simulation of free surface flow around a ship in calm water. It is a Lagrangian and meshless particle scheme which is applied to the projection method for the incompressible governing equations. This requires the solution of Poisson problems in each time step, so a moving least squares (MLS) interpolants is used for the spatial derivatives in order to discretize the Poisson equation with pressure-Dirichlet condition of free surface flow in meshless structure. Meanwhile, an additional problem of the periodic particle locations redistribution in the present approach is still handled by MLS interpolants. With the proposed FPM technique, problems associated with the free surface flow around a ship are circumvented. A verification of numerical modeling is made using the Wigley hull and the validity of the proposed methodology is examined by comparing the detail of wave profile and wave-making resistance with Series 60 model. The results demonstrate that FPM is able to perform efficient and stable simulations of free surface flow around a ship.

Keywords Lagrangian · Finite pointset method (FPM) · Projection method · Moving least squares (MLS) · Free surface flow · Wave-making resistance

✉ Yu Lu
luyu90627@126.com

[1] College of Shipbuilding Engineering, Harbin Engineering University, Harbin 150001, China

[2] CIMC Ocean Engineering Design & Research Institute Co., Ltd, Shanghai 201206, China

1 Introduction

Meshless techniques or particle methods have become quite prevalent in computational mechanics. The key point of these methods is to supply numerical solutions with a set of arbitrarily distributed points without using any mesh to link them. Compared to traditional mesh techniques that consume time and simulate difficultly for some problems with large deformation or within complicated geometry, particle methods are found to be appropriate and acceptable.

Smoothed particle hydrodynamics (SPH) is the longest established free Lagrangian method and is quickly approaching a mature stage among the various meshless methods. Development of this classical meshless method has increased during the last decades, SPH which was originally used for the treatment of astrophysical phenomena [1, 2] has been extensively studied, extended and applied to varieties of engineering problems so far. From the view of naval architecture, a detailed discussion of the relevant mesh-free method and its connections to predict ship motions for a Wigley hull was presented in Pearce et al. [3]. Daniel and Tim [4] combined strip theory and SPH algorithm for solving the problem of ship keel and bow-flare slamming. The $2D + t$ approach has been introduced into SPH computations to study the ship-breaking wave pattern by Marrone et al. [5]. Following the $2D + t$ method, Landrini et al. [6, 7] developed a hybrid analysis and application of BEM-SPH used for simulating the free surface bow flow around a high speed ship. Compared to the classical mesh-based method, although SPH has a number of advantages in terms of the harmonious combination of the Lagrangian formulation and particle approximation, the adaptive nature for modeling complex free surfaces without the need of any form of

explicit surface tracking [8] and so on, this type of meshless method has suffered several numerical drawbacks: inconsistency, and difficulty in the treatment of boundary conditions. Several methods developed to improve SPH have been presented in ref [9–12]. Other detailed discussion on SPH method modification can be found in [13–16].

On the other hand, Finite point method (FPM) proposed by Oñate et al. [17–19] is the representative example of meshless method which has been developed for fluid mechanics problems. This approach is implemented in such a way that finite number of particles (pointset) which are so-called numerical grid points and can be arbitrarily distributed consist of the fluid domain and use different least square interpolation scheme within each point cloud to minimize the distance between the interpolated function and the value of the unknown point. As a result, the discrete equations as well as point redistribution are obtained in that way. Moreover, the particles in Finite point method merely participant in interpolation for the field information. Compared to the classical SPH method, this makes the method easier in terms of numerical implementation and more flexible for the treatment of boundaries by just prescribing boundary conditions on points placed on boundaries naturally as well as particle management. It is found that FPM is suitable to handle, for example, flow problems with complicated and rapidly changing geometry [20], free surface flows [21, 22] and multiphase flows [23, 24].

A main focus of this paper lies on the application of the Finite pointset method to the incompressible and inviscid governing equations. Therefore, we propose numerical simulation of free surface flow around a ship moving with a constant speed in calm water based on FPM. The incompressibility is taken care of by a projection method. This requires the solution of Poisson problems in each time step. Thereupon, the approximation of spatial derivatives arisen from pressure Poisson equation is obtained by the moving least squares (MLS) interpolants. When it comes to the use of MLS on particle methods, it should be noted that though this interpolation scheme has several superiorities such as the regularity and accuracy of the solution, the permission of avoiding some stability control corrections, it may also lead to the loss of conservation properties and a general robustness reduction of the scheme as a sacrifice [25, 26]. As for the treatment of boundary conditions, we place the boundary particles at all domain boundaries to satisfy Neumann boundary condition. Since the particle positions are given by a scattered point cloud changes from time step to time step, it is in need of an efficient data management or re-meshing technique to process the problems associated with irregular particle distribution during flow. Regarding the treatment of free surface, a concept of particle density is chosen as the judgment criteria to distinguish the point on free surface by time step. Through comparing the detail of wave profile and wave-making resistance of experiment with Lagrangian finite pointset method numerical simulation, the proposed methodology demonstrate the capability of FPM as a meshless method for accurate and robust simulation of incompressible fluid flows.

The paper is organized as follows. In Sect. 2, we describe the implementation of FPM in detail, which contains the mathematical model governing the incompressible flow of fluid, the moving least square (MLS) approximation and the projection method for solving the following discretization of Poisson equation, the point redistribution or data management, and the free surface treatment. In Sect. 3, a verification of numerical modeling is made using the Wigley hull and the validity of the proposed methodology is examined by comparing the detail of wave profile and wave-making resistance with Series 60 model. The paper ends up with concluding remarks in Sect. 4.

2 Implementation of FPM

2.1 Governing equations

The equations of fluid mechanics are derived from physical balance and conservation principles by assuming the fluid to be a continuum and the quantities being sufficiently smooth. In a Lagrangian frame, the mass and momentum conservation equations for the motion of a viscous incompressible can be written as

Mass conservation:

$$\frac{\mathrm{D}\rho}{\mathrm{D}t} + \rho\frac{\partial u_i}{\partial x_i} = 0 \tag{1}$$

Momentum conservation (RANS turbulent model):

$$\rho\frac{\mathrm{Du_i}}{\mathrm{D}t} + \rho\frac{\partial\left(u_j u_i + \overline{u_j'' u_i''}\right)}{\partial x_j} = -\frac{\partial p}{\partial x_i} + \frac{\partial}{\partial x_i}\left(\mu\left(\frac{\partial u_i}{\partial x_j} + \frac{\partial u_j}{\partial x_i}\right)\right) + \rho\bar{f}_i \tag{2}$$

where $\bar{}$ is time average physical components, $''$ is time fluctuating physical components, $\rho\overline{u_j'' u_i''}$ is Reynolds stress tensor, and ρ is the fluid density, t the time, u_i the Cartesian ith components of the velocity field, x_i the Cartesian ith components of the position vector, p the pressure, μ the viscosity and f_i the source term (normally the gravity g_i). $\mathrm{D}\varphi/\mathrm{D}t$ denotes the total or material time derivative of a function φ.

From the view of the potential flow theory, the well-known Rankine source method is proposed by Dawson [27] and then has been widely applied as a classical method for solving some practical problems. In addition, many

improvements containing the consideration of the nonlinearity of the free surface physics have been conducted by the researchers who are Musker [28], Nakos and Sclavounos [29], Millward et al. [30] and so on. Therefore, these improved approaches have deeply demonstrated that when dealing with the free surface flow around a ship neglecting viscosity is a classical and practical method and can also give a satisfactory and valid result. Since the main focus of this paper is the ship wave-making resistance which is obtained by the surface particle pressure integration, so based on the same assumption as the popular Rankine source method in potential theory, we suppose the fluid be of no viscosity so that the arising viscosity term μ and the time average physical term in Eq. (2) can be neglected. For this condition of incompressible fluid potential flow, Eqs. (1) and (2) can be, respectively, simplified as:

$$\frac{\partial u_i}{\partial x_i} = 0 \tag{3}$$

$$\rho \frac{\mathrm{Du_i}}{\mathrm{D}t} = -\frac{\partial p}{\partial x_i} + \rho g_i \tag{4}$$

where the source term f_i is replaced by the gravity g_i.

2.2 The projection method

In FPM, we consider the projection method [31] to solve the Eqs. (3) and (4) in time. A semi-implicit method is employed. The momentum conservation equation is firstly explicitly solved to obtain the temporal velocities and positions except the pressure gradient term

$$r_i^{n+1} = r_i^n + \Delta t u_i^n \tag{5}$$

$$\tilde{u}_i^{n+1} = u_i^n + \Delta t g_i \tag{6}$$

where r_i^n is the Cartesian ith components of the particle position vector, and the left hand side of Eq. (6) $\tilde{u}_i^{n+1}$ is the intermediate velocity term.

Then the pressure is calculated implicitly with the following Poisson equation of pressure deduced from the mass conservation equation to maintain the incompressibility of the fluid. That is:

$$u_i^{n+1} = \tilde{u}_i^{n+1} - \frac{\Delta t}{\rho} \frac{\partial p^{n+1}}{\partial x_i} \tag{7}$$

where the pressure gradient is added. Meanwhile, the new arising velocity must fulfill the incompressibility constraint

$$\frac{\partial u_i^{n+1}}{\partial x_i} = 0 \tag{8}$$

Such that velocity gradient ∇u^{n+1} in Eq. (8). This yields a Poisson equation for the pressure p^{n+1} to be solved

$$\frac{\partial}{\partial x_i}\left(\frac{\partial p^{n+1}}{\partial x_j}\right) = \frac{\rho}{\Delta t}\frac{\partial \tilde{u}_i^{n+1}}{\partial x_i} \tag{9}$$

For the boundary condition, in which case the boundary particles move along the solid wall, so the velocity on the boundary Γ can be formulated as:

$$\vec{u} \cdot \vec{n} = 0 \quad \text{and} \quad \frac{\partial \vec{u}}{\partial \vec{n}} \cdot t = 0 \quad \forall t \cdot \vec{n} = 0 \tag{10}$$

where $\vec{n}$ is the wall unit normal vector, i.e., there is no velocity component into or away from the wall. In this case the Neumann boundary condition for pressure on Γ is derived as

$$\left(\frac{\partial p}{\partial \vec{n}}\right)^{n+1} = \mu \frac{\partial}{\partial x_i}\left(\frac{\partial u_i^n}{\partial x_j}\right)\vec{n} + \rho g \vec{n} \tag{11}$$

As for the kinematic and dynamic boundary conditions on free surface, it can then be obtained by the equations for the free surface potential φ and for the position of free surface particles which are implemented as follows:

$$\frac{\mathrm{D}\varphi}{\mathrm{D}t} = \frac{1}{2}|\nabla\varphi|^2 - g\eta, \quad \frac{\mathrm{Dx_i}}{\mathrm{D}t} = \nabla\varphi, \quad p^* = 0 \tag{12}$$

where η represents the vertical position of the considered free surface particle, p^* is the pressure of the particles detected on the free surface boundary. Incidentally, note that in the particles method both dynamic and kinematic free surface boundary conditions are intrinsically satisfied as proved by Colagrossi et al. [32].

In this projection method, the particle positions are updated only in the first step. The intermediate velocity, the pressure and the final divergence free velocity are all computed on the new particle positions. The spatial derivatives appearing in the above equations are approximated by the moving least squares (MLS) which will directly be used to discretize Poisson pressure Eq. (9). As computing this second-order systems of equation over time which will bring about numerical damping associated with the time-stepping schemes, the scheme adopted in this paper maintains first-order accuracy. Meantime, the pressure-Dirichlet boundary condition on the free surface is satisfied by simply prescribing the pressures on the corresponding boundary points to the fixed values. Eventually, we use this mathematical model to numerical simulate the free surface flow around a ship.

2.3 Moving least square approximation function

The Moving Least Squares (MLS) was used for reconstructing a function from values given at scattered data points. It locally best approximates the function in some polynomial basis, weighted with respect to the interpolation point. While the polynomial basis remains fixed, the

weights move over the computational domain Ω, thus the method is also referred to as moving weighted least squares (MWLS) method. Due to the weights changing over the domain, the global approximating function is not a polynomial. The method is used as a building block for approximation function in the interpolating case.

Let a function u be given on a domain $\Omega \subset R^d$. Consider a point cloud $X = \{x_1, \ldots, x_n\}$. The function values $u_1, \ldots, u_n$ are given at the data points by $u_i = u(x_i)$. The task is to approximate the function value $u(x)$ at an arbitrary point $x \in \Omega$, i.e., in the first place we are confronted with a meshless interpolation problem.

The first step of the MLS is to assign weights to the points x_i via a distance weight function w. Analysis of the MLS is often times carried out for a class of global distance weight functions. The distance weight function is chosen smooth and decaying with increasing distance. If one wishes to have strictly compactly supported distance weight functions, one often chooses

$$w(d) = \begin{cases} \exp(-(d^2 - h^2)^{-2}) & d < h \\ 0 & d \geq h \end{cases} \tag{13}$$

or splines

$$w(d) = \begin{cases} 1 - 6\left(\frac{d}{h}\right)^2 + 8\left(\frac{d}{h}\right)^3 - 3\left(\frac{d}{h}\right)^4 & d < h \\ 0 & d \geq h \end{cases} \tag{14}$$

where $d = |x - x_i|$ is a positive distance between any two particles in Euclidian norm, since it is rotationally invariant. The size of the searching radius h determines n, the number of neighboring particles around x to be used for MLS approximation. In this paper, the searching radius h is obtained by referencing the work of Koshizuka and Oka [33], and decided by numerical debugging constantly in computation.

Let P_v express the vector space of polynomials up to order v. Consider a basis $(b_0, \ldots, b_k)$ of this vector space. In this paper, for P_3 in 3D one can consider the canonical basis

$$\begin{aligned} &b_0(x,y,z) = 1, \quad b_1(x,y,z) = x, \quad b_2(x,y,z) = y, \\ &b_3(x,y,z) = z, \quad b_4(x,y,z) = x^2, \\ &b_5(x,y,z) = xy, \quad b_6(x,y,z) = y^2, \quad b_7(x,y,z) = yz, \\ &b_8(x,y,z) = z^2, \quad b_9(x,y,z) = xz \end{aligned} \tag{15}$$

And then any polynomial $p \in P_v$ can be written as

$$p(x) = \sum_{j=0}^{k} a_j b_j(x) = b(x)^T \cdot a \tag{16}$$

with basis vector $b(x) = (b_0(x), \ldots, b_k(x))^T$ and coefficient vector $a = (a_0, \ldots, a_k)^T$. A specific point $\hat{x}$ is considered and the functional

$$E_{\hat{x}}(a) = \sum_{i=0}^{n} w_i(\hat{x})(p(x_i) - u_i)^2 \tag{17}$$

is minimized, i.e., one selects the polynomial $p \in P_v$, defined by the coefficient vector a, which minimizes the moving least squares distance at the data points x_i. Since the weights w_i are taken with respect to the point $\hat{x}$, for every point $\hat{x}$ one obtains a different polynomial, and thus a different coefficient vector $a(\hat{x})$.

The coefficient vector $a(\hat{x})$ is obtained by the normal equations

$$(VW(\hat{x})V^T)a(\hat{x}) = (VW(\hat{x}))u \tag{18}$$

where

$$\begin{aligned} V &= \begin{pmatrix} b_0(x_1) & \ldots & b_0(x_n) \\ \vdots & \ddots & \vdots \\ b_k(x_1) & \cdots & b_k(x_n) \end{pmatrix} \in R^{(k+1)\times n} \quad \text{and} \\ W &= \begin{pmatrix} w_1(\hat{x}) & & \\ & \ddots & \\ & & w_n(\hat{x}) \end{pmatrix} \in R^{n\times n} \end{aligned} \tag{19}$$

Hence, for each point $\hat{x}$ a small linear system bas to be solved with matrix $VW(\hat{x})V^T \in R^{(k+1)\times(k+1)}$. For every point $\hat{x}$ one has a polynomial approximation

$$\Pi u(x) = p_x(x) = b(x)^T \cdot a(x) \tag{20}$$

Finally, the operator Π acts on a function u and yields a new function which is constructed only from the values of u at the data points of the cloud X. It is noteworthy that the MLS approximation can be used only if the points adopted are not too disordered otherwise the matrices can be ill-conditioned. This is a problem encountered by some authors using the meshless method in the context of breaking waves or for large free surface deformations (see, e.g., [26]).

2.4 Point data management

Meshless methods, in particular particle methods, for which the point cloud changes from time step to time step, require a fair amount of data management to be efficient. In this subsection, we outline the ideas required to obtain efficient methods.

The point data management mainly involves finding neighboring points, removing close points and filling holes among the flow domain bestrewed by a finite number of particles (or points) participating in interpolation and discretization. Tree search algorithm [34] is used for searching neighboring points since this technique works well for problems with variable radius h_i. In this paper, for obtaining more point data information around the ship on the free surface but reducing unnecessary numerical

simulation time in balance, we use variable radius h which is kept at a low value 0.05 near the ship and then rises with the distance rate 0.2 away from there until it reaches a given maximum value 0.3, and then stays at this level. Numerical tests show that the tree search method is very efficient and robust especially for large number of particles of variable radius [35].

When finding some points' shortest distances closer than a given distance $d_{\min}$ by looping over all points, removing close points by the method of interpolating using all neighboring points is worth effort. It is implemented in such a way that let the detected two particles for too close have the positions $\vec{x}_k$ and $\vec{x}_l$, and the corresponding data vectors $\vec{u}_k$ and $\vec{u}_l$, so the new inserted particle will be in the center of mass of the two particles and interpolate linearly in the data which is $\vec{x} = (\vec{x}_k + \vec{x}_k)/2$, and $\vec{u} = (\vec{u}_k + \vec{u}_k)/2$, respectively. As for the condition with too largest holes generating during flow, searching for all the Voronoi cell [36] of point x_i in 2D or in 3D and constructing the full Voronoi diagram [37] are the core missions. Once those largest holes are identified by Voronoi diagrams, new points will be inserted and participant calculation. It is known that when dealing with the problem of point re-distributions by the Voronoi diagram, this can inevitably introduce a "mesh" ingredient in their scheme. However, taking into consideration of the construction of spatial derivatives which are evaluated through MLS, this proposed particle approach, to a large extent, should be classified as a meshless method.

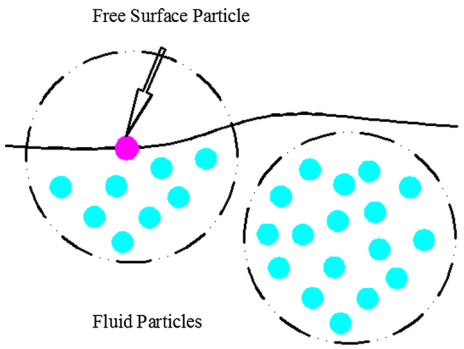

Fig. 1 Points clouds in free surface and flow domain

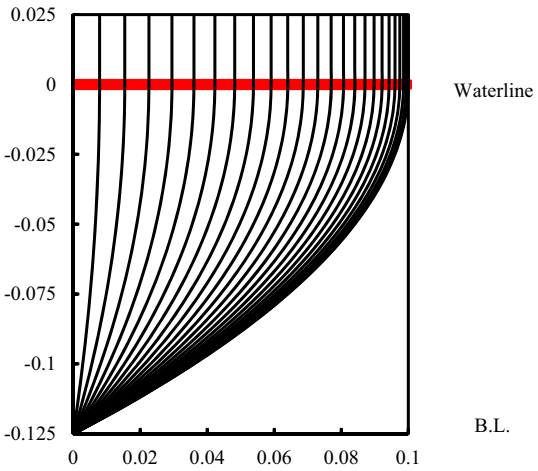

Fig. 2 The half body plan (symmetry) of the Wigley hull

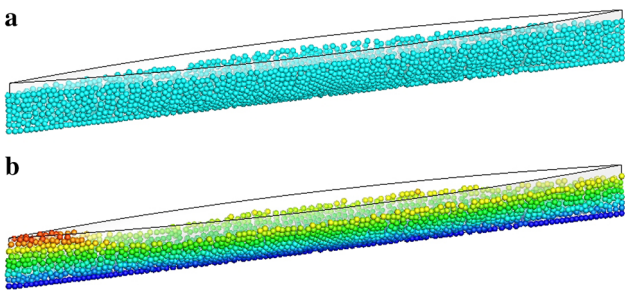

Fig. 3 The distribution of particles over the Wigley hull at respective initial time **a** and finished time **b** for the condition of $F_n = 0.316$

2.5 Free surface treatment

As for the numerical simulation of free surface flow, the treatment of free surface flow has always been considered and developed into some practicable ideas. Dilts [38] proposed a purely geometric exposure method to detect corresponding boundary particles, which eliminates the limitations of the summation method [39] and does not rely on the particular interpolant used. Marrone et al. [40] introduced a more precise and reliable controlling concept which is based on the properties of the SPH kernel to complete the free surface detection. In this paper, we adopt "particle density" [41, 42] as the judgment criteria to distinguish the point on free surface boundary. It is done by introducing a formula for free surface index, which is defined as:

$$\langle n \rangle_i = \sum_{i=1}^{n} w(|\boldsymbol{r} - \boldsymbol{r}_i|) \tag{21}$$

where w is the distance weight function proposed above. See Fig. 1, since there is no fluid points outside the free

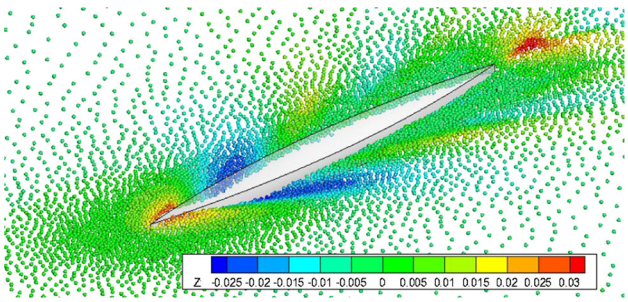

Fig. 4 Scattered points on the free surface at $F_n = 0.316$

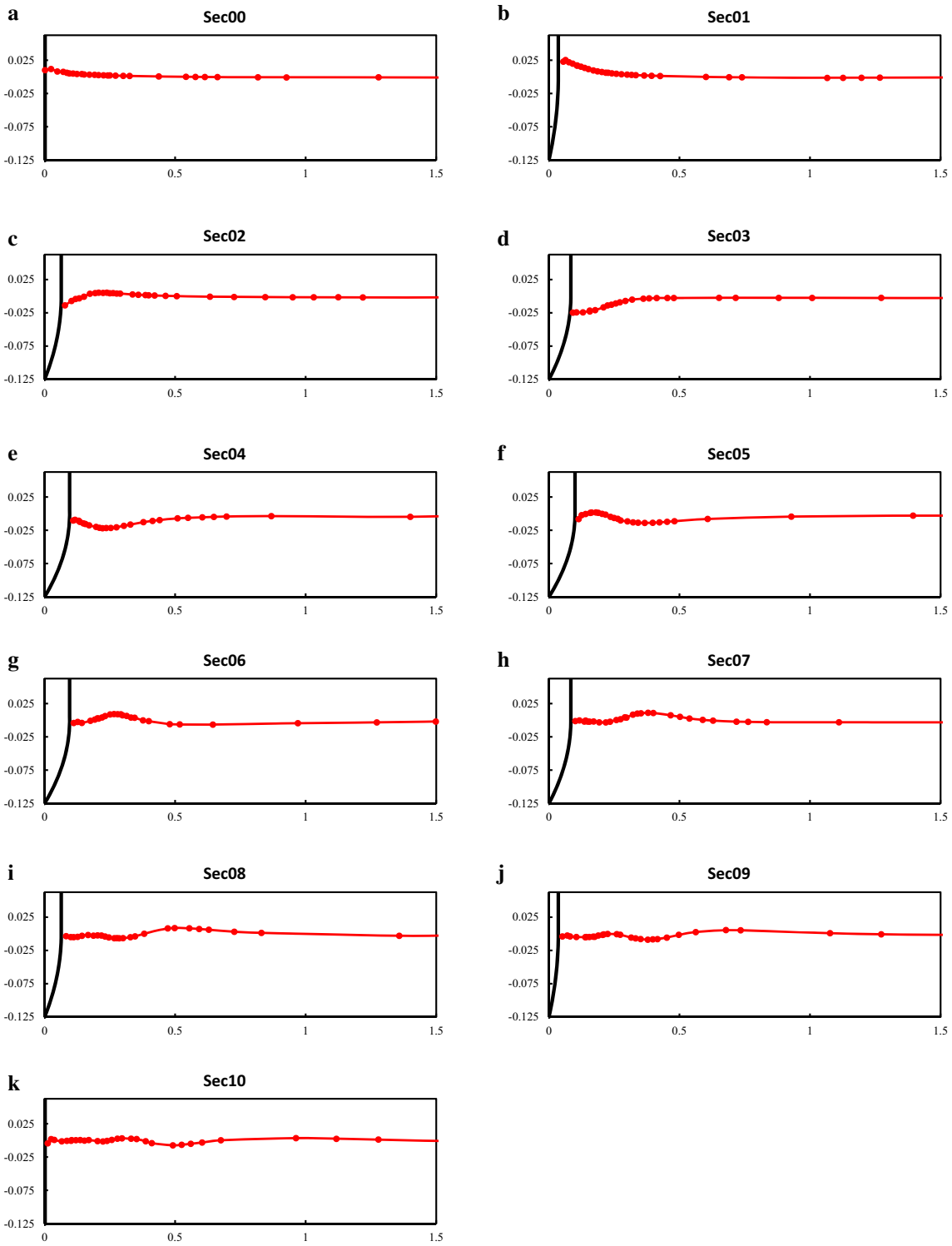

Fig. 5 Transvers wave cuts profiles of the Wigley hull in various sections at $F_n = 0.316$. **a** Wave profile at $x = -1$, named Sec00. **b** Wave profile at $x = -0.8$, named Sec01. **c** Wave profile at $x = -0.6$, named Sec02. **d** Wave profile at $x = -0.4$, named Sec03. **e** Wave profile at $x = -0.2$, named Sec04. **f** Wave profile at $x = 0$, named Sec05. **g** Wave profile at $x = 0.2$, named Sec06. **h** Wave profile at $x = 0.4$, named Sec07. **i** Wave profile at $x = 0.6$, named Sec08 **j** Wave profile at $x = 0.8$, named Sec09. **k** Wave profile at $x = 1$, named Sec10

surface boundary Γ, which will result in the one's index satisfying the criterion, i.e., $\langle n \rangle_i < \beta \cdot n^0$. n^0 denotes the free surface index value of an particle inside the fluid domain Ω at the initial stage, and β is an free surface parameter assumed 0.80–0.99 in this paper. So we can identify free surface boundary particles in this way.

2.6 Time step selection

In order to obtain numerical stability, several time step constraints should satisfied where it includes a Courant–Friedrichs–Lewy (CFL) condition,

$$\Delta t \leq 0.12 \frac{h}{U_{\max}} \tag{22}$$

where $U_{\max}$ denotes the maximum velocity under the given condition. As the hydrodynamical force acting on the particle g_i, the additional constraints is added,

$$\Delta t \leq 0.24 \min_{\forall a} \sqrt{\frac{h}{g_i}} \tag{23}$$

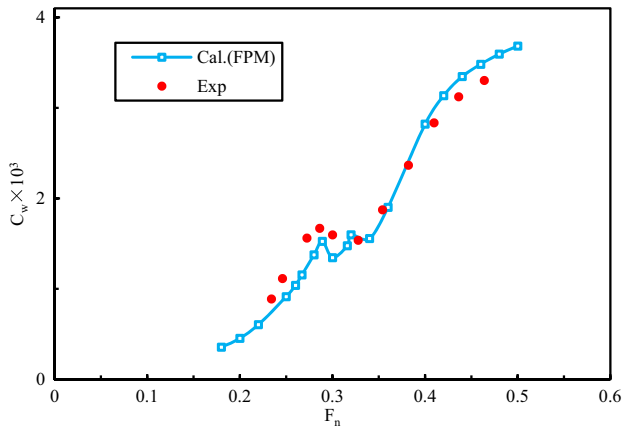

Fig. 6 Wave-making resistance of the Wigley hull

3 Numerical results and discussions

In this section, we apply the FPM outlined in the preceding sections to the prediction of wave-making resistance and wave profiles (longitudinal and transverse wave cuts) for two hull models at a wide range of Froude numbers. The wave drag R_w is computed by integrating the particle pressure p over the ship wetted surface S projecting to the Cartesian x-axis direction $\vec{n}_x$ which is opposed to the direction of ship progressing. That is $R_w = \int_s p\vec{n}_x d\vec{s}$. With the time iteration going during the computation, the calculating pressure consequently will reach a satisfying numerical stable state, and output a final steady-state value. And then, the wave resistance coefficient can be determined by $C_w = \frac{R_w}{1/2\rho U^2 S}$, where U is the ship velocity in calm water corresponding to the Froude number.

For the first problem, the well-known Wigley hull model is considered which is defined by the analytical formula

$$y = \frac{B}{2}\left[1 - \left(\frac{2x}{L}\right)^2\right]\left[1 - \left(\frac{z}{T}\right)^2\right] \tag{24}$$

where L, B and T are the length, breadth and draft of the ship, respectively, at still water. The characteristic dimensions of the Wigley hull are $B/L = 0.1$, $T/L = 0.0625$, $CB = 0.444$, and $L = 2$ m, while the depth of 3D computational domain size is 1.4 m and the initial time increment is set 0.001 s in this paper. In Fig. 2, the half body plan (symmetry) is shown while in Fig. 3 we drew the particles arrangement over the ship model at calculation initial time and finished time (or steady time), respectively,

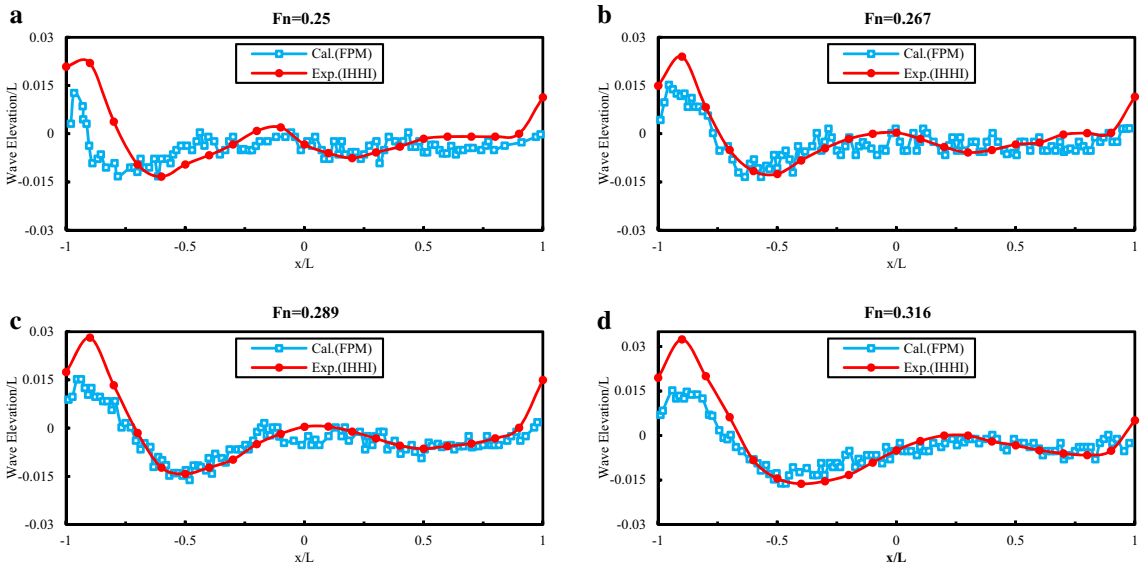

Fig. 7 Wave profile along the Wigley hull at various Froude numbers. **a** Wave profile at $F_n = 0.25$. **b** wave profile at $F_n = 0.267$. **c** Wave profile at $F_n = 0.289$ and **d** wave profile $F_n = 0.316$

at $F_n = 0.316$. Note that there are nearly 2.0×10^5 particles in flow domain.

In the case of $F_n = 0.316$, the wave counters plotted by tracking the scattered spatial coordinates of points on the free surface ($z = 0$ in still water) are presented in Fig. 4.

Figure 5 presents the transverse wave cuts profiles for the case with $F_n = 0.316$ in multi-sections which ordered from 'Sec00' at ship stem to 'Sec10' at hull stern. Note that in the present work, the wave elevation in draught direction around the Wigley hull is tracked by the particles positions on free surface.

In Fig. 6, the computed wave-making co-efficient of the Wigley hull with fixed sinkage and trim is compared with its experimental results [43]. It can be observed that the results of calculation are in good agreement with the test data.

Figure 7 shows a comparison of computed and measured wave profile at various speed of the Wigley hull in fixed sinkage and trim condition. It can be seen that the wave phases are nearly consistent, but in the case of low Froude value, such as $F_n = 0.25$, a significant difference is found at the stem region of hull, and the phase moved forward relative to the experimental wave profile. Though the first wave crest values are generally less than experiment, with the Froude value increasing, the values of first wave trough are consistent to the test results, what's more, the rest waveforms along the ship hull have satisfier agreements. When analyzing the reason why the computed bow wave is underpredicted throughout the range of Froude values, the intrinsic numerical damping of the scheme accepted may be an influence factor. Thus, it is possible to try different spatial resolution to improve this numerical scheme in further study, but not in this paper.

The following validation studies are carried out for the Series 60 ship, $C_B = 0.6$ and $L = 2$ m hull model, with fixed sinkage and trim. The body plan of the Series 60 ship is shown in Fig. 8. At $Fr = 0.316$, the principal view of the wave counter for Series 60 hull in form of spatial particles

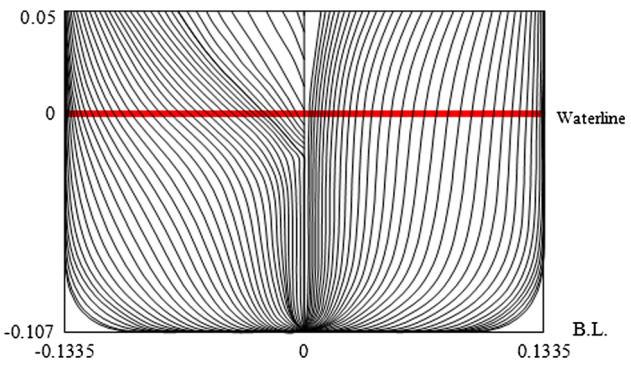

Fig. 8 The body plan of the Series 60 ship

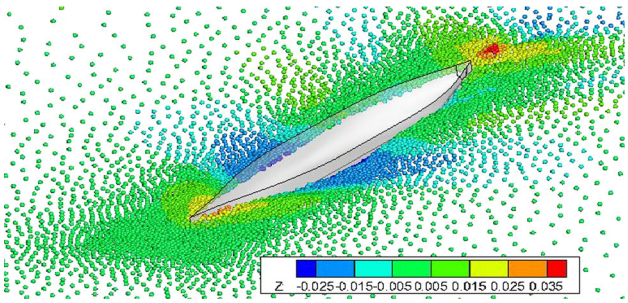

Fig. 9 The particles arrangement over the Series 60 ship at finished time with $F_n = 0.316$

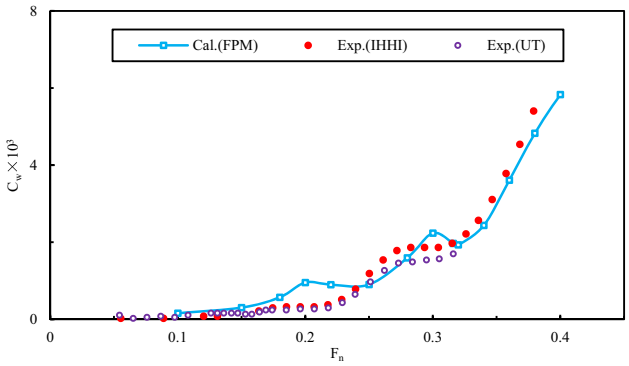

Fig. 10 Wave-making resistance of the Series 60 ship

scattered about the free surface ($z = 0$ in still water) is shown in Fig. 9.

The comparison between the calculated wave-making resistance coefficients by present method and the experimental measurements which are obtained by the University of Tokyo (UT) and Ishikawajima-Harima Heavy Industries Co., Ltd. (IHHI) are plotted in Fig. 10.

Under the condition of fixed sinkage and trim, the predicted wave profiles along the Series 60 hull at various Froude numbers are compared with the experimental results [44] by the Ship Research Institute (SRI) in Fig. 11. As shown in Fig. 11, the agreement with the experimental data is in general good except the condition with low Froude numbers. This phenomenon is same to that of Wigley hull. When $F_n = 0.18$ in wave profiles, some large fluctuations occurred around the experimental measurements along the Series 60 hull. Note that ζ is Wave Elevation in Fig. 11. It should be noted that the spiky fluctuations in Figs. 7 and 11 may be blamed on the reason that the wave elevation and complicated deformation on the free surface lead to incontinuity and nonhomogeneity of particles. This will inevitably result in some fluctuations between the adjacent two particles. Even though, the wave plots along the length of shipboard still clearly demonstrate the discipline of wave profile variation and the validity by comparing with the experimental data.

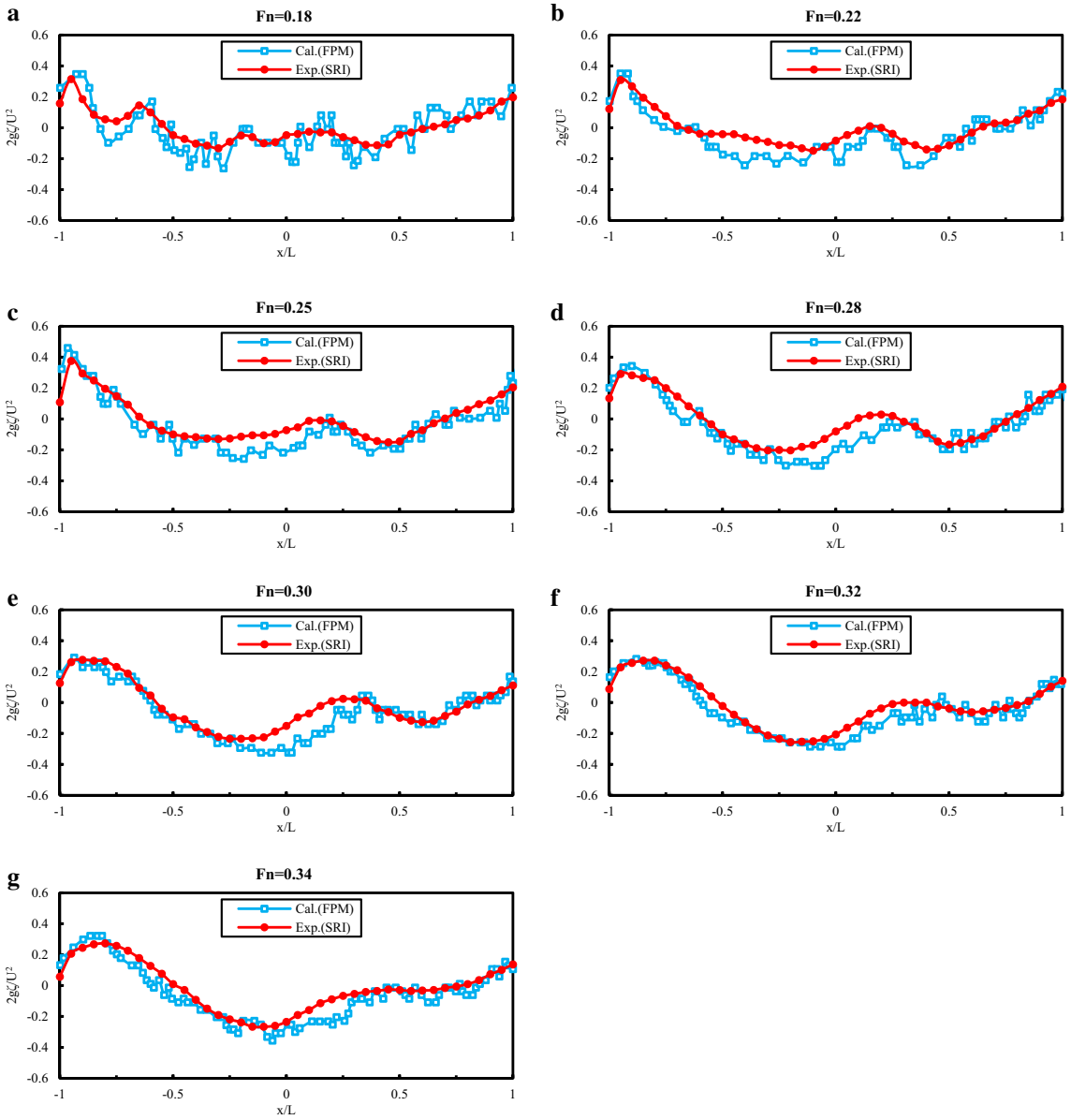

Fig. 11 Wave profile along the Series 60 ship at various Froude numbers. **a** Wave profile at $F_n = 0.18$. **b** Wave profile at $F_n = 0.22$. **c** Wave profile at $F_n = 0.25$. **d** Wave profile $F_n = 0.28$. **e** Wave profile at $F_n = 0.30$. **f** Wave profile at $F_n = 0.32$. **g** Wave profile $F_n = 0.34$

Comparison is done in Fig. 12 between the calculated longitudinal wave cuts profiles at multi-values of y/L with different x/L locations and the measurements in the case of $F_n = 0.316$. Take notice that the experiment results are acquired from the work by Toda et al. [45]. As can be seen that the agreement is quite satisfactory, especially the interval from the stem to stern ($-1 \leq x/L \leq 1$). Several discrepancies are only found at the zone which is located at $x/L \geq 1.5$, behind the hull stern position.

In Fig. 13, we list the numerical results of wave pattern on the free surface under multi-conditions of Froude numbers in both display forms which contain the one plotted by scatter points (left), i.e., the participating calculation particles, and the other drawn by counters (right). From these figures, we can discover that the stern region is full of vortices, and the maximum wave crest and trough around the hull swell with the increase of Froude numbers markedly. The two type pictures shall both predict the

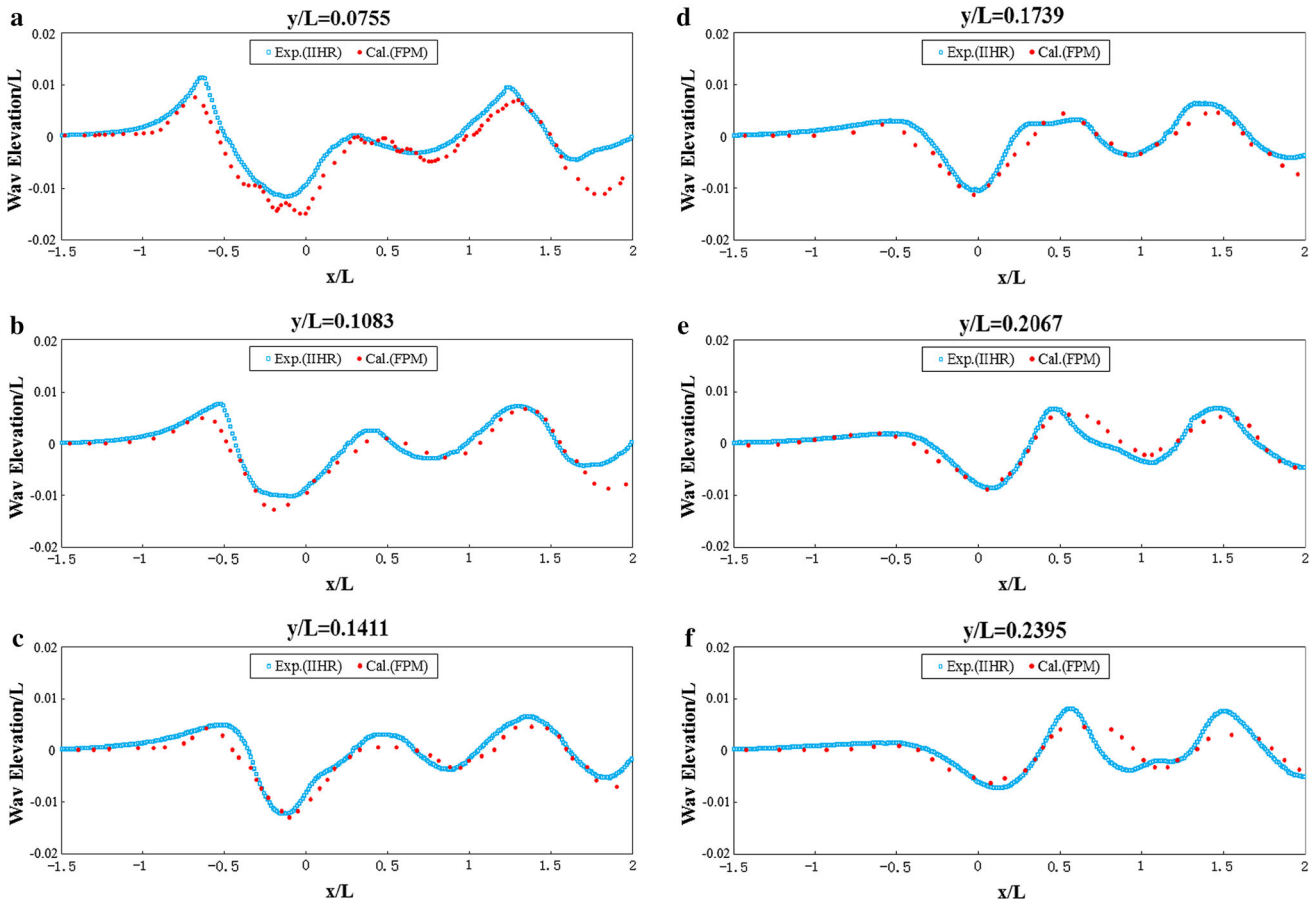

Fig. 12 Longitudinal wave cuts profiles of the Series 60 ship at different values of y/L under the condition of $F_n = 0.316$. **a** Wave profile at $y/L = 0.0755$. **b** Wave profile at $y/L = 0.1083$. **c** Wave profile at $y/L = 0.1411$. **d** Wave profile at $y/L = 0.1739$. **e** Wave profile at $y/L = 0.2067$. **f** Wave profile at $y/L = 0.2395$

wave distributions on free surface around a moving ship accurately.

4 Conclusions

The paper represents a Finite pointset method (FPM) for applying to simulate the free surface flow around a ship propagating in calm water. By adopting the projection method to fulfill the incompressibility of flow, meanwhile introducing the moving least squares (MLS) interpolants for solving the pressure Poisson equation, we obtain an efficient solution for the problems associated with free surface flow. Particles data management for overcoming irregular particle distribution and the treatment of free surface are both considered during flow calculation.

Validation studies have been implemented for the Wigley hull as well as Series 60 model. The comparison between calculated results and experimental data shows a quite satisfy agreement except a few discrepancies arising in the case of low Froude numbers. In general, it is indicated that FPM is an efficient and robust numerical method for evaluating the flow field, wave pattern and wave-making resistance for practical ship forms.

The calculated results are influenced to a certain degree by the rules of local particles refinement around the hull

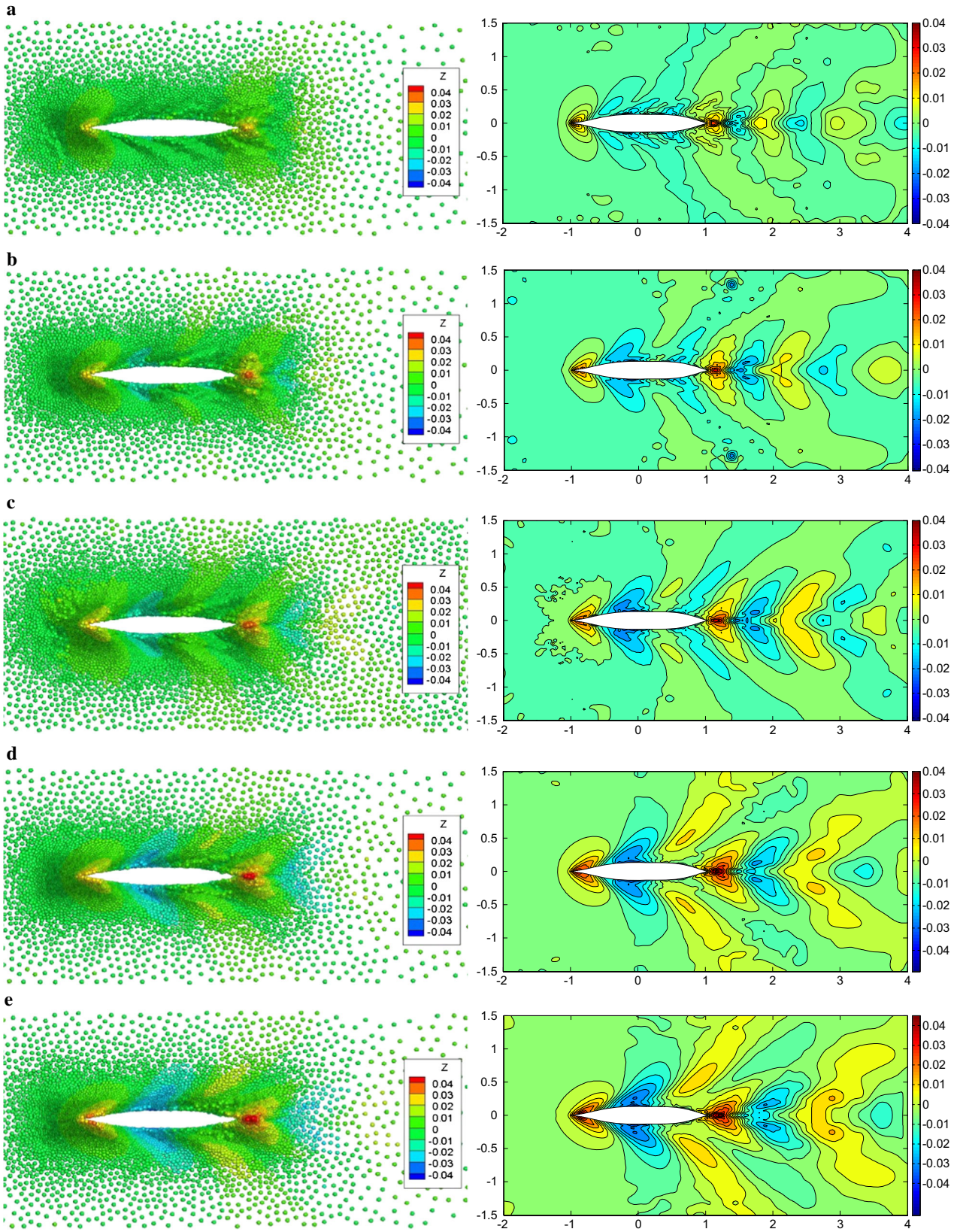

Fig. 13 Wave patterns in two displayed forms including scatter points (*left*) and counters (*right*) at various Froude numbers. **a** Wave pattern at $F_n = 0.25$. **b** Wave pattern at $F_n = 0.28$. **c** Wave pattern at $F_n = 0.30$. **d** Wave pattern at $F_n = 0.32$. **e** Wave pattern at $F_n = 0.34$

and the number of particles in calculation domain during numerical simulating. Hence, some investigations on calculation accuracy should be further studied.

Acknowledgments We would like to thank the National Natural Science Foundation of China (Grant No. 51379040) for the financial support of our research.

References

1. Lucy LB (1977) A numerical approach to the testing of the fission hypothesis. Astron J 82:1013–1024
2. Gingold RA, Monaghan JJ (1977) Smoothed particle hydrodynamics: theory and application to non-spherical stars. Mon Not R Astron Soc 181(3):375–389
3. Pearce M, Takeda T, Hudson D (2011) Prediction of ship motions for a Wigley Hull. In: Proceedings of 6th international SPHERIC workshop, Germany, Hamburg, June, pp 226–232
4. Veen D, Gourlay T (2012) A combined strip theory and smoothed particle hydrodynamics approach for estimating slamming loads on a ship in head seas. Ocean Eng 43:64–71
5. Marrone S, Colagrossi A, Antuono M, Lugni C, Tulin MP (2011) A 2D+t SPH model to study the breaking wave pattern generated by fast ships. J Fluids Struct 27(8):1199–1215
6. Landrini M, Colagrossi A, Tulin MP (2001) Breaking bow and stern waves: numerical simulations. In: Proceedings of 16th international Workshop on water waves and floating bodies, Japan, Hiroshima
7. Landrini M, Colagrossi A, Greco M, Tulin MP (2012) The fluid mechanics of splashing bow waves on ships: a hybrid BEM–SPH analysis. Ocean Eng 53:111–127
8. Wan DC, Shen ZR, Ma J (2010) Numerical simulations of viscous flows around surface ship by level set method. J Hydrodyn Ser B 22(5):271–277
9. Chen JK, Beraun JE (2000) A generalized smoothed particle hydrodynamics method for nonlinear dynamic problems. Comput Methods Appl Mech Eng 190(1):225–239
10. Johnson GR, Beissel SR (1996) Normalized smoothing functions for SPH impact computations. Int J Numer Meth Eng 39(16):2725–2741
11. Bonet J, Lok TS (1999) Variational and momentum preservation aspects of smooth particle hydrodynamic formulations. Comput Methods Appl Mech Eng 180(1):97–115
12. Fang J, Parriaux A, Rentschler M, Ancey C (2009) Improved SPH methods for simulating free surface flows of viscous fluids. Appl Numer Math 59(2):251–271
13. Zhang GM, Batra RC (2004) Modified smoothed particle hydrodynamics method and its application to transient problems. Comput Mech 34(2):137–146
14. Liu WK, Jun S, Zhang YF (1995) Reproducing kernel particle methods. Int J Numer Meth Fluids 20(8–9):1081–1106
15. Liu MB, Xie WP, Liu GR (2005) Modeling incompressible flows using a finite particle method. Appl Math Model 29(12):1252–1270
16. Oger G, Doring M, Alessandrini B, Ferrant P (2007) An improved SPH method: towards higher order convergence. J Comput Phys 225(2):1472–1492
17. Oñate E, Idelsohn S, Zienkiewicz OC, Taylor RL (1996) A finite point method in computational mechanics. Applications to convective transport and fluid flow. Int J Numer Methods Eng 39(22):3839–3866
18. Oñate E, Idelsohn S, Zienkiewicz OC, Taylor RL, Sacco C (1996) A stabilized finite point method for analysis of fluid mechanics problems. Comput Methods Appl Mech Eng 139(1):315–346
19. Zienkiewicz OC, Oñate E, Idelsohn S (1995) Moving least square approximations for solution of differential equations. Centro Internacional de Métodos Numéricos en Ingeniería, Spain
20. Kuhnert J, Tramecon A, Ullrich P (2000) Advanced air bag fluid structure coupled simulations applied to out-of position cases. In: EUROPAM conference proceedings, Paris
21. Tiwari S, Kuhnert J (2002) A meshfree method for incompressible fluid flows with incorporated surface tension. Revue Européenne des Éléments 11(7–8):965–987
22. Tiwari S, Kuhnert J (2003) Particle method for simulation of free surface flows. Hyperbolic problems: theory, numerics applications. Springer, Berlin, Heidelberg, pp 889–898
23. Hietel D, Junk M, Kuhnert J, Tiwari S (2005) Meshless methods for conservation laws. Analysis and numerics for conservation laws. Springer, Berlin, Heidelberg, pp 339–362
24. Tiwari S, Kuhnert J (2005) A numerical scheme for solving incompressible and low mach number flows by the finite pointset method. Meshfree methods for partial differential equations II. Springer, Berlin, Heidelberg, pp 191–206
25. Dilts GA (1999) Moving-least-squares-particle hydrodynamics—I. Consistency and stability. Int J Numer Meth Eng 44(8):1115–1155
26. Le Touzé D, Colagrossi A, Colicchio G, Greco M (2013) A critical investigation of smoothed particle hydrodynamics applied to problems with free-surfaces. Int J Numer Meth Fluids 73(7):660–691
27. Dawson CW (1977) A practical computer method for solving ship-wave problems. In: Proceedings of the 2nd international conference on numerical ship hydrodynamics, Berkeley, CA, pp 30–38
28. Musker AJ (1989) A panel method for predicting ship wave resistance. In: 17th symposium on naval hydrodynamics, pp 143–150
29. Nakos DE, Sclavounos PD (1994) Kelvin Wakes and wave resistance of cruiser and transom-stern ships. J Ship Res 38(1):9–29
30. Millward A, Nicolaou D, Rigby SG (2003) Numerical modelling of the water flow around a fast ship with a transom stern. Int J Marit Eng 145(A3):21–34
31. Chorin A (1968) Numerical solution of the Navier–Stokes equations. J Math Comput 22:745–762
32. Colagrossi A, Antuono M, LeTouze D (2009) Theoretical considerations on the free surface role in the SPH model. Phys Rev E Stat Nonlinear Soft Mater Phys 79(5):056701 **(:1-13)**
33. Koshizuka S, Oka Y (1996) Moving-particle semi-implicit method for fragmentation of incompressible fluid. Nucl Sci Eng 123(3):421–434
34. Beasley JE, Cao B (1996) A tree search algorithm for the crew scheduling problem. Eur J Oper Res 94(3):517–526
35. Hernquist L, Katz N (1989) TREESPH-A unification of SPH with the hierarchical tree method. Astrophys J Suppl Ser 70:419–446
36. Voronoi G (1908) Nouvelles applications des paramètres continus à la théorie des formes quadratiques. Premier mémoire. Sur quelques propriétés des formes quadratiques positives parfaites. Journal für die reine und angewandte Mathematik 133:97–178
37. Fortune S (1987) A sweepline algorithm for Voronoi diagrams. Algorithmica 2(1–4):153–174
38. Dilts GA (2000) Moving least-squares particle hydrodynamics II: conservation and boundaries. Int J Numer Meth Eng 48(10):1503–1524
39. Randles PW, Libersky LD (1996) Smoothed particle hydrodynamics: some recent improvements and applications. Comput Methods Appl Mech Eng 139(1):375–408
40. Marrone S, Colagrossi A, Le Touzé D, Graziani G (2010) Fast free-surface detection and level-set function definition in SPH solvers. J Comput Phys 229(10):3652–3663

41. Shibata K, Koshizuka S (2007) Numerical analysis of shipping water impact on a deck using a particle method. Ocean Eng 34(3–4):585–593
42. Shibata K, Koshizuka S, Sakai M, Tanizawa K (2012) Lagrangian simulations of ship-wave interactions in rough seas. Ocean Eng 42:13–25
43. Shearer JR, Cross JJ (1965) The experimental determination of the components of ship resistance for a mathematical model. Trans RINA 107:459–473
44. Takeshi H, Hino T, Hinatsu M, Tsukada Y, Fujisawa J (1987) ITTC cooperative experiments on Series 60 model at Ship research institute–flow measurements and resistance tests. Ship Res Inst Japan (Papers), 1–48
45. Toda Y, Stern F, Longo J (1992) Mean-flow measurements in the boundary layer and wake and wave field of a series 60 CB = 0.6 ship model-Part 1: Froude numbers 0.16 and 0.316. IIHR Report No 352